Integrating Multi-Sensing Technology for Preemptive Detection of Highway Slope Instability

Rakesh Salunke, Ph.D.[1]; Rahul Biswas[2]; Sadik Khan, Ph.D., P.E.[3]; and Ian La Cour[4]

[1]Postdoctoral Research Scientist, Dept. of Civil and Environmental Engineering, Jackson State Univ., Jackson, MS. Email: rakesh.salunke@jsums.edu
[2]Graduate Research Assistant, Dept. of Civil and Environmental Engineering, Jackson State Univ., Jackson, MS. Email: rahul.biswas@students.jsums.edu
[3]Associate Professor, Dept. of Civil and Environmental Engineering, Jackson State Univ., Jackson, MS. Email: sadik.khan@jsums.edu
[4]Materials Division, Mississippi Dept. of Transportation, Jackson, MS.
Email: ilacour@mdot.ms.gov

Downloaded from ascelibrary.org by A Q M Zohuruzzaman on 04/23/25. Copyright ASCE. For personal use only; all rights reserved.

ABSTRACT

Highway slopes are susceptible to various geohazards, including landslides, rockfalls, and soil creep, necessitating early detection to minimize disruptions, prevent collisions, and ensure road safety. Conventional methods, such as visual inspections and periodic surveys, may overlook subtle changes or fail to provide timely alerts. This research aims to enhance slope movement and instability detection by leveraging advanced remote-sensing technologies such as interferometric synthetic aperture radar (InSAR), light detection and ranging (LiDAR), and uncrewed aerial vehicles (UAV). The primary objective is to develop an integrated approach combining multiple data sources to detect and predict highway slope movement effectively. InSAR offers surface deformation measurements over time, capturing nuanced slope movements, while LiDAR and UAVs provide high-resolution elevation information, including slope angles, curvature, and vegetation cover. This study explores methods to integrate these complementary data sets to validate the slope movement detection from InSAR. The research involves establishing a baseline ground motion scenario using historical open-access Sentinel-1 satellite data spanning 10 years (2018–2024) for the central Mississippi region, characterized by expansive clay prone to volume changes, then comparing the ground motions with those observed from near-surface remote sensing. The baseline ground motion scenario is compared with ground truthing from near-surface remote sensing surveys conducted by LiDAR and UAV photogrammetry. The point cloud and imagery obtained from LiDAR and UAVs facilitated cross-verification and validation of the InSAR ground displacements. This study provides a comprehensive and innovative methodology for monitoring highway infrastructure using InSAR and near-surface remote sensing techniques such as LiDAR and UAV. Continuous ground motion analysis provides immediate feedback on slope performance, helping to prevent potential failures. LiDAR change detection allows for detailed evaluation of highway slopes and precise identification of potential failure locations. Integrating remote sensing techniques into geotechnical asset management programs is crucial for proactively assessing risks and enhancing highway safety and resilience. Future studies will use this data set to create finite-element-based numerical models, aiding in developing surrogate models for highway embankments based on observed InSAR ground motion patterns. This study will also serve as a foundation for future machine-learning classification models for detecting vulnerable geo-infrastructure assets.

© ASCE

Downloaded from ascelibrary.org by A Q M Zohuruzzaman on 04/23/25. Copyright ASCE. For personal use only; all rights reserved.

INTRODUCTION

Various remote sensing technologies, including satellite-based radar, can detect surface displacement with millimeter-level accuracy, allowing highway slope monitoring. Interferometric Synthetic Aperture Radar (InSAR), a widely used surface deformation detection tool, achieves submillimeter accuracy. It identifies scatterers across target areas without the use of ground monitoring stations, allowing for extensive surveillance with precise sub-millimeter displacement measurement accuracy. Field validation confirms InSAR's ability to achieve sub-millimeter accuracy in both vertical and horizontal directions, making it ideal for tracking slow movements. Space-borne synthetic aperture radar (SAR) instruments, particularly InSAR, allow accurate measurement of land deformation by analyzing phase differences in complex SAR images taken at different times. InSAR emerges as a cutting-edge tool capable of large-scale reconnaissance and detailed monitoring. Several industrial case studies demonstrate its effectiveness in assessing landslide and slope stability (Akcin et al., 2010; Herrera et al., 2010). InSAR is a technique that exploits the phase difference between two complex SAR images captured at different times (Fruneau et al., 1996; Massonnet & Feigl, 1998). Using phase information, relative distances can be measured accurately to within a fraction of a wavelength. Deformation mapping using InSAR has been proven capable of giving relative 'line of sight' (LOS) deformation measurements with accuracy of the order of millimeters– centimeters (Lauknes, 2004). Lately, the concept of combining InSAR information from many SAR images, thus allowing the creation of a deformation time series, has been introduced (Berardino et al., 2002; Ferretti et al., 2001). Although InSAR is a valuable tool for ground deformation detection, it is important to validate with ground truth information.

In this study, digital elevation models (DEM) developed from Light Detection and Ranging (LiDAR) point clouds and uncrewed aerial vehicles (UAV) photogrammetry were used for InSAR ground displacement validation. LiDAR is a remote sensing technology that computes distances to objects by measuring the time for laser beams to reflect and return from the objects. LiDAR is similar to radar but uses laser light instead of radio waves. Changes in the properties of the light help in determining the properties of the Earth's surface (Chan et al., 2007). LiDAR can measure the Earth's surface rapidly, producing a dense point cloud used to create 3D representations. LiDAR often operates in the near-infrared spectrum, but some systems use the green band to penetrate water for bathymetric mapping. LiDAR-derived elevations are highly accurate, with recent data having absolute accuracies of 10 to 20 centimeters and even better relative accuracies.

Highway slopes in Mississippi are prone to shallow slope failures due to factors such as the abundance of expansive clay soil in the region combined with the wetting and drying weather cycles. Volumetric changes experienced by the expansive clay due to moisture variation damage essential geo-infrastructure assets over time. The geo-infrastructure assets impacted include highway embankments and slopes that support roads, bridges, railroads, and other critical civil infrastructure. Preemptive detection of ground displacement and slope instabilities is imperative to tailor the maintenance of these critical infrastructure assets. Manual, boots-on-ground inspection of thousands of miles of highway embankments and slopes across the state are labor intensive, inefficient, and impractical.

Therefore, this study proposes implementing InSAR to detect ground deformation of highway slopes and compare and validate with UAV and LiDAR ground deformation results. InSAR imagery in the region of interest in Mississippi (MS) were used for a broad preliminary

analysis of displacements and compared with slope movements observed from high-resolution UAV and LiDAR-based DEMs.

METHODOLOGY

The methodology began with data collection of Sentinel-1 satellite data, followed by preprocessing using the Sentinel Application Platform (SNAP) software. Preprocessing steps included coregistration, interferogram generation, error and noise reduction, phase unwrapping, geocoding and terrain correction, and validation. Terrestrial LiDAR data collected for one year at the study sites were then compared with the outcome of the InSAR analysis. The methodology schematic is presented in Figure 1. Ground deformation was derived from InSAR data processing and analysis, then validated by comparing the deformation results at two highway embankment side slopes in Jackson, MS. Two highway embankment side slopes were selected to validate the ground motion. Slope 1 (located along the I20W exit toward Terry Road) and Slope 2 (located along I220W near McRaven Road). The slope site locations are presented in Figure 2.

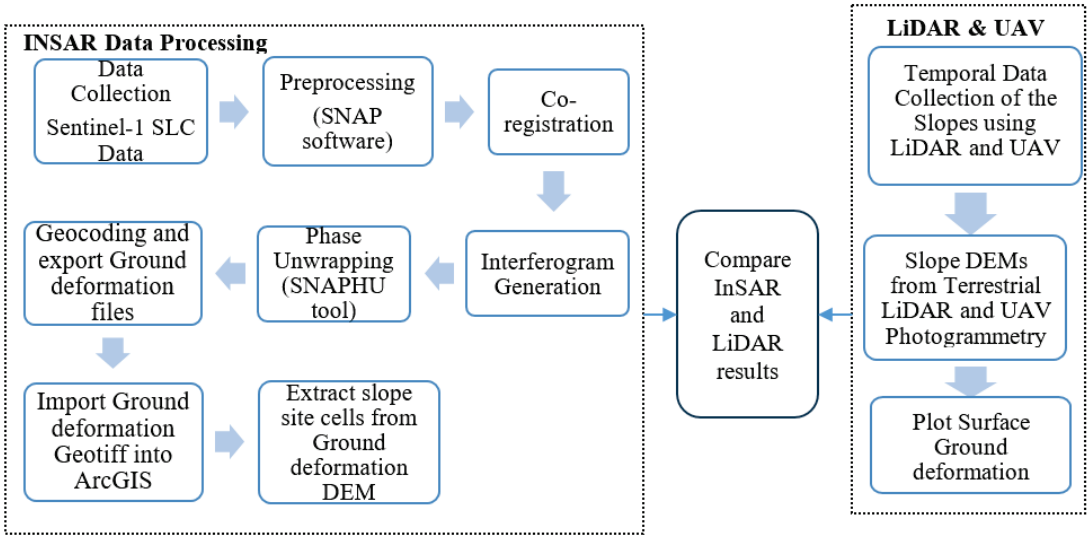

Figure 1. Methodology schematic describing InSAR analysis and validation workflow

Figure 2. Slope 1 and Slope 2 locations with near-surface remote sensing data

Downloaded from ascelibrary.org by A Q M Zohuruzzaman on 04/23/25. Copyright ASCE. For personal use only; all rights reserved.

Downloaded from ascelibrary.org by A Q M Zohuruzzaman on 04/23/25. Copyright ASCE. For personal use only; all rights reserved.

INSAR Data Collection & Processing

The Sentinel 1A-based InSAR data was processed using SNAP software, and interferograms were generated. Sentinel-1 IW SLC images dated April 11, 2018, and April 15, 2024, were collected from the European Space Agency (ESA) Copernicus Open Access Hub. The key properties of the InSAR dataset are summarized in Table 1. A sample global coverage of Sentinel-1 SLC products as of May 2020 is provided in Figure 3.

Table 1. Properties of InSAR Data

Acquisition Date	11th April 2018	15th April 2024
Orbit Cycle	136	319
Average Scene Height (m)	70.33	70.43
Satellite Mission	Sentinel-1A	
Passage direction	Ascending (South to North)	
Product type	SLC	
Pixel Spacing: Range x Azimuth [m]	2.33 x 13.94	
Acquisition Mode	IW	

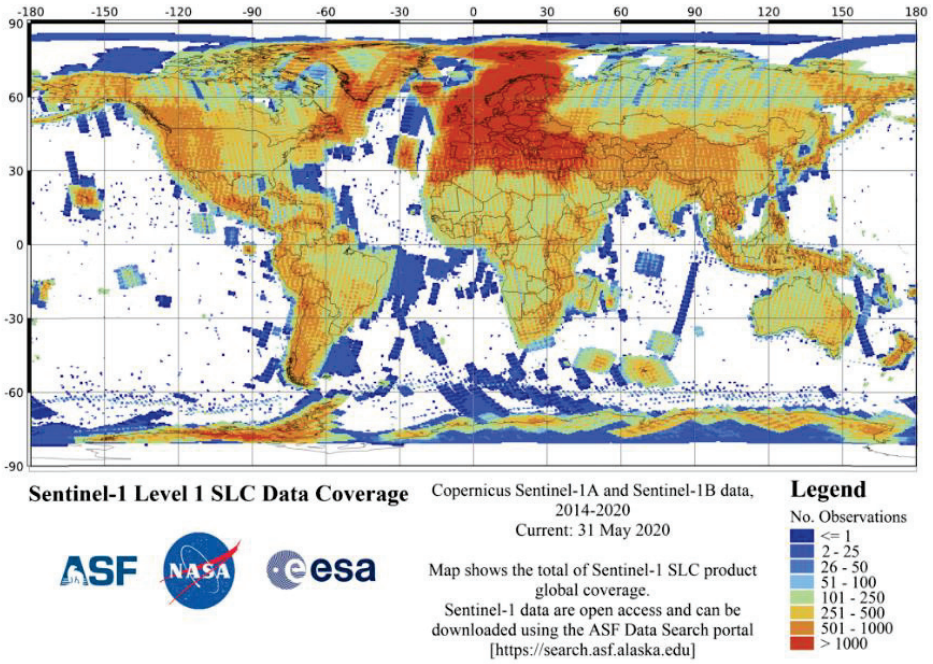

Figure 3. Global coverage of Sentinel-1 SLC products as of May 2020. *Source: https://search.asf.Alaska.edu*

Sentinel-1 IW mode captures data by dividing the total swath (coverage area) into three sub-swaths: IW1, IW2, IW3. Each sub-swath corresponds to a different range of incidence angles and collectively covers a broad area on the ground. In InSAR analysis, the sub-swaths ensure the SAR images of the area of interest are compared in an interferogram and come from the same

Downloaded from ascelibrary.org by A Q M Zohuruzzaman on 04/23/25. Copyright ASCE. For personal use only; all rights reserved.

sub-swath consistency. Within each sub-swath, Sentinel-1 uses bursts, which are smaller segments of data. Each sub-swath is further divided into bursts of data. In processing data, extracting corresponding bursts from multiple acquisitions is crucial to avoid decorrelation. Specification of bursts is necessary for a specific area to perform different steps of data analysis in SNAP, such as TOP-SAR-Split or Applying Earth Orbit. Specific sub-swaths and bursts were selected from the Sentinel- Single Look Complex (SLC) data to focus on the area of interest in Mississippi, thus reducing the data size and conserving download and processing time. After data collection, preprocessing was performed, beginning with the coregisrtation.

Coregistration. The SLC pairs were coregistered to ensure precise alignment between the reference and secondary images. This step was crucial to accurately measure surface deformation by comparing images taken at different times. Orbit files were applied to correct the SAR data using precise orbit information, ensuring accurate geolocation and alignment by applying updated satellite position and velocity data. Back geocoding was performed to align multiple SAR images to a common reference image, ensuring that pixels representing the same ground location in different images were correctly aligned, which is essential for interferometric analysis.

Interferogram Generation. Interferograms were generated from the coregistered SLC pairs, showing the phase difference between the co-registered SAR images. This phase difference is key to detecting ground motion. The TOPSAR deburst tool was used to merge individual bursts within each sub-swath into a continuous image, eliminating burst discontinuities to create a seamless interferogram.

Error and Noise Reduction. The SAR images were then multilooked to reduce speckle noise and improve the radiometric quality of the SAR image. Goldstein phase filtering was applied to the interferogram to reduce phase noise and enhance signal quality, ensuring robust phase unwrapping.

Phase Unwrapping. Phase unwrapping was performed using the Statistical-Cost Network-Flow Algorithm for phase unwrapping (SNAPHU). The filtered interferogram was prepared and exported using an export tool for phase unwrapping. The wrapped phase values were converted into continuous phase values in SNAPHU, which were critical for creating a ground movement model. The interferogram development snapshots for MS are presented in Figure 4.

Geocoding and Terrain Correction. The unwrapped phase images were geocoded to map the displacement results onto geographic coordinates. This involved transforming radar coordinates into a standard geographic coordinate system. Terrain correction was applied to compensate for distortions due to topographic variations and the inclination of the satellite sensor, ensuring an accurate geometric representation of the images.

Validation. The InSAR results were validated using ground truth data and other complementary data sources to ensure the accuracy and reliability of the InSAR-derived displacement measurements. By following these steps, a comprehensive and accurate assessment of surface deformation was achieved, providing valuable insights into the stability and movement of the monitored area.

The next stage of the InSAR analysis was carried out in ArcGIS. The DEM (raster) output with vertical ground displacement from SNAP was exported as a georeferenced file and imported into ArcGIS for further visualization and analysis. The ground displacement from InSAR images between 2-18 and 2024 were then compared with the ground displacement observed using high-resolution UAV and LiDAR data on the two study slope sites.

Downloaded from ascelibrary.org by A Q M Zohuruzzaman on 04/23/25. Copyright ASCE. For personal use only; all rights reserved.

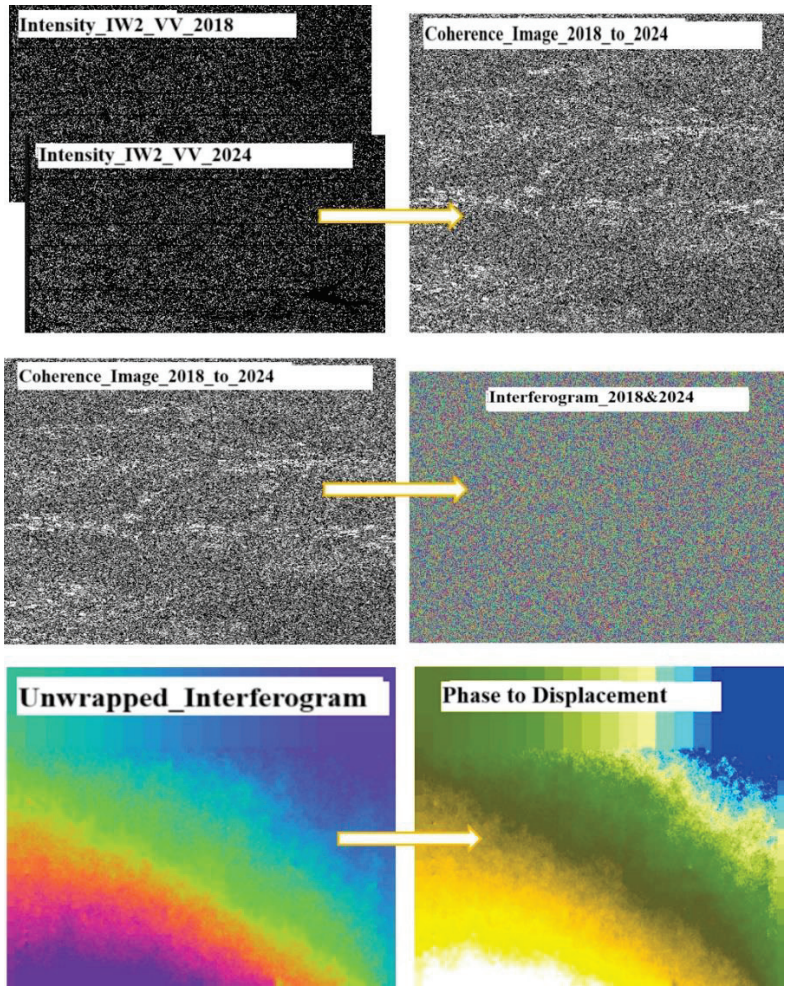

Figure 4. InSAR data analysis workflow in SNAP

Near-surface Remote Sensing workflow using UAV and LiDAR

Aerial optical and thermal imagery from the two slope sites were captured using a DJI-Matrice 200 drone operated by an FAA Part 107 licensed pilot. The drone's integrated 3-axis gimbal stabilized the camera, reducing blur. Flights were conducted at 100 to 200 ft (30–60 m) using manufacturer-recommended mobile applications for planning and control. The gimbal's pitch range was adjustable from −90° (nadir) to +30°. A Zenmuse-XT2 Dual Sensor camera, featuring an optical camera and a FLIR thermal sensor, was used to capture the images. A 70% - 80% overlap between the shots was maintained to ensure a high-quality orthomosaic and 3D model. Markers were placed at known ground control points to aid georeferencing during post-processing. Raw Image processing and georeferencing were performed in Simactive Correlator 3D software to develop orthomosaics and 3D Models.

Terrestrial LiDAR equipment (Trimble X7) was used to perform 3D laser scanning of the selected embankment slopes at different times over two years. The scanner was placed at four to ten stations along the slope to scan distressed areas. The self-leveling scanner indicated proper alignment within -10 to +10 degrees with solid green lights. Up to ten spherical targets 4 feet above the ground were set up to aid in post-processing the point cloud data. Field scan data were

recorded using "Trimble Perspective" software on a handheld tablet (Trimble T10X). The scanner was moved between stations following the manufacturer's instructions, ensuring sufficient overlap (around 30 to 65 feet apart) for good scan registration. Calibration was automatically initiated with each scan, correcting collimation errors and ensuring accurate measurements without manual adjustments.

DEM and surface profile creation workflow

The slope point clouds captured from LiDAR surveys were georeferenced using ground control points with known MS state plane coordinates, allowing for the superimposition of point clouds collected at different time intervals. Raw point clouds were segmented to remove unwanted edge points, and a ground extraction algorithm was applied to eliminate vegetation and above-surface points, leaving only bare ground points. The bare ground point clouds from all seasons were imported into Civil 3D, and digital elevation models or surfaces were developed using the triangular irregular network (TIN) method. The georeferenced point clouds and surfaces were geolocated using the MS state plane coordinate system, processed in Autodesk software, and then mapped using Microsoft Corporation, Maxar, CNES, and Airbus DS data. Seasonal topographic surfaces were superimposed to identify variations. Multidirectional alignments were created along the slope. Comparative analyses of surface profiles and resistivity imaging data provided insights into soil movement and subsurface moisture changes due to weather patterns.

ANALYSIS AND RESULTS

Ground Displacement. The full-phase representation of topographic variations of SAR data analysis in SNAP was exported as a ground displacement raster and imported into ArcGIS Pro. The raster units were adjusted from meters to feet using the raster calculation tool within ArcGIS Pro. The ground displacement between 2018 (baseline) and 2024 for the central MS region plotted in ArcGIS is presented in Figure 5a. Then the InSAR vertical ground displacement raster was clipped to extract the area of interest at slope 1 -I20 WB Terry Road and slope 2 -I220N and I55N interchange are presented in Figures 5b and 5c, respectively. The negative values in the line of site displacement values presented in Figure 5 indicate the movement away from the sensor or subsidence, and the positive values indicate the movement towards the sensor, or uplift when the satellite's line of sight is ascending(South to North). Slopes 1 and 2 both show positive values, and given the ascending(South to North) line of sight of the Sentinel -1 imagery used for InSAR analysis, the positive displacement values mean uplift. The average ground displacements obtained by averaging cell values in Slopes 1 and 2 (Figure 5b & c) are 0.40' and 0.79', respectively.

LiDAR & UAV Results

The InSAR ground displacement results from the two study slope sites were compared with the surface displacements observed from high-res LiDAR and UAV DEMs. DEMs obtained from UAV surveys in Summer 2021 and Fall 2022 for Slope 1 are presented in Figure 6 (a) and (b), respectively, followed by the 3D model representations in Figure 6 (c) and (d). The DEM obtained from LiDAR point cloud surveys, along with the slope surface profile variations, are

Downloaded from ascelibrary.org by A Q M Zohuruzzaman on 04/23/25. Copyright ASCE. For personal use only; all rights reserved.

presented in Figure 6 (e), (f), and (g), respectively. From the high-res DEM, the average displacement observed for surface profile B-B' on Slope 1 is 0.07'. The average displacement between summer 2021 and fall 2022 for Slope 2 = 0.12'

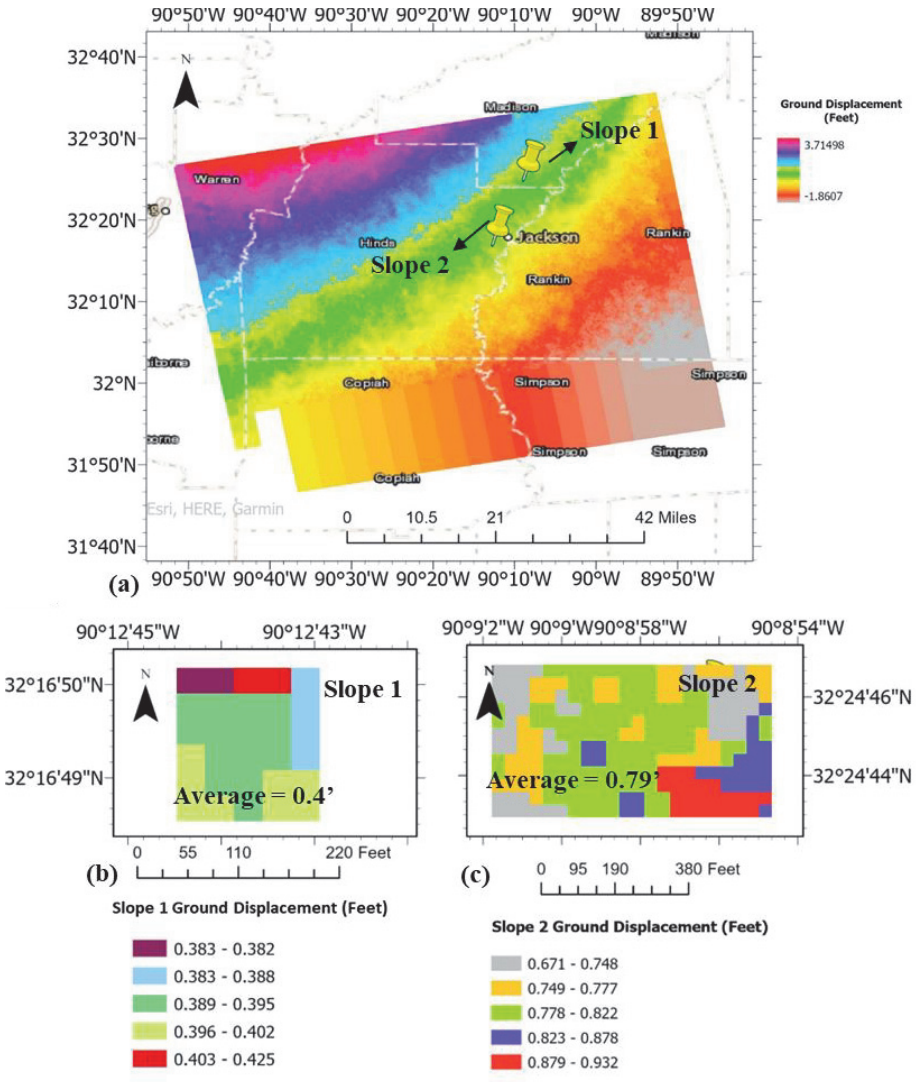

Figure 5. InSAR ground displacement between 2018 (baseline) and 2024 (plotted in ArcGIS) (a) Central MS (b) Study area Slope 1 -I20 WB Terry Road (c) Study area Slope 2 -I220N and I55N interchange

Comparison of vertical ground motion between InSAR and LiDAR

The average ground displacement values obtained from InSAR analysis for Slope 1 over seven years was 0.40' (yearly average 0.06'), and for Slope 2 was 0.79' (yearly average 0.11'). The ground displacements observed from high resolution LiDAR and UAV DEM data are presented in Table 2. Between summer 2021 and Fall 2022, an average displacement of 0.07' (settlement) was observed in Slope 1. For slope 2, an average displacement of 0.12' (uplift) was observed within the span of 1 year.

Downloaded from ascelibrary.org by A Q M Zohuruzzaman on 04/23/25. Copyright ASCE. For personal use only; all rights reserved.

Downloaded from ascelibrary.org by A Q M Zohuruzzaman on 04/23/25. Copyright ASCE. For personal use only; all rights reserved.

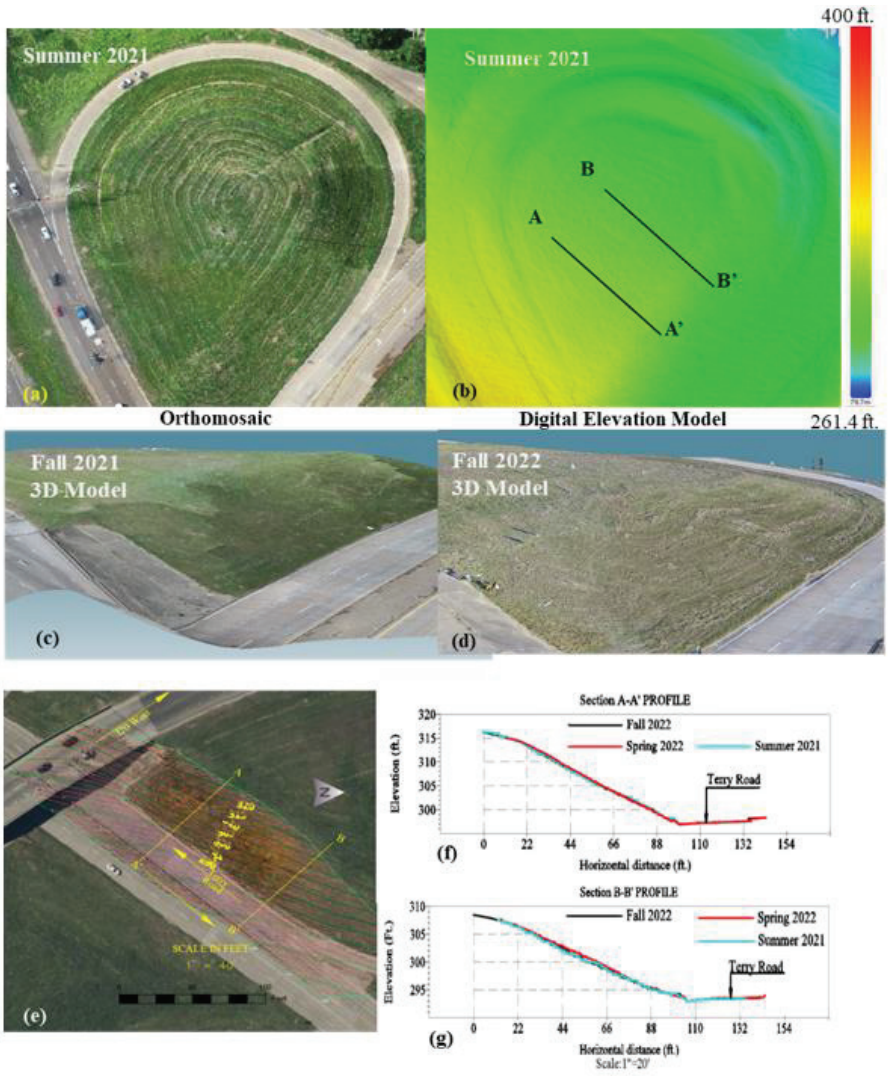

Figure 6. Sample UAV and LiDAR DEM and vertical ground motion results for Slope 1 (a) (b) (c) (d) (e) (*Similar results available for Slope 2 and not shown due to space constraint)*

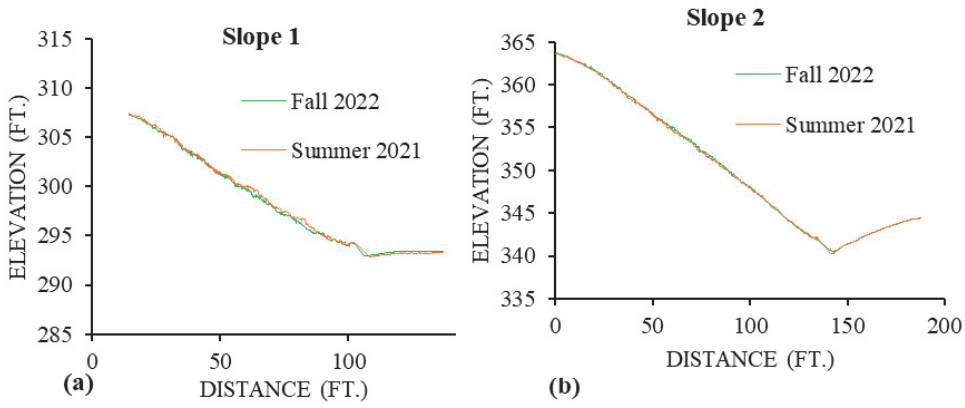

Figure 7. Surface Profile Variation from LiDAR Results

© ASCE

Downloaded from ascelibrary.org by A Q M Zohuruzzaman on 04/23/25. Copyright ASCE. For personal use only; all rights reserved.

Table 2. Annual ground displacements observed from LiDAR data

	LiDAR Displacement (ft.)			
Distance (Ft.)	**Slope 1**	**Remarks**	**Slope 2**	**Remarks**
20	-0.32	uplift	-0.08	uplift
40	-0.12	uplift	-0.27	uplift
60	0.17	settlement	-0.33	uplift
80	0.31	settlement	-0.19	uplift
100	0.42	settlement	0.05	settlement
120	-0.06	uplift	0.11	settlement
Average	**0.07'**		**-0.12'**	

DISCUSSION & CONCLUSIONS

This paper focuses on determining the efficacy of using InSAR, validated by UAV and LiDAR DEM measurements, to monitor geo-infrastructure assets and preemptively detect threats from excess ground displacements. The validation of InSAR ground displacements from LiDAR and UAV results performed in this study will pave the way for implementing remote sensing technology for geotechnical asset management. Continuous ground motion analysis provides immediate feedback about how the slopes are performing and how to avoid potential failure even before it happens. LiDAR change detection allows detailed evaluation of highway way slopes and precise identification of the potential failure location.

The line-of-sight displacement obtained from InSAR images provides information on ground movement, indicating horizontal or vertical displacement. Positive values indicate movement towards the sensor, suggesting either north-to-south or upward movement. Conversely, negative values indicate movement away from the sensor, which could mean south-to-north or downward movement. In our observations from InSAR analysis, most or all pixel values were positive for both slopes, suggesting movement from south to north or uplift.

The average ground displacement values calculated from cell statistics for 6 years were 0.38' for Slope 1 and 0.75' for Slope 2, indicating uplift and South to North translational movement. Considering a yearly displacement of 0.07', the total displacement over the period of 6 years is 0.42' for Slope 1 and 0.82' for Slope 2, which are comparable to the results observed in the corresponding InSAR images of 0.38' for Slope 1 and 0.75' for slope 2. The uplift movement was observed from LiDAR measurements for Slope 2, matching that from the InSAR analysis, whereas the average displacement from lidar results for Slope 1 indicated settlement. The upheavals and subsidences could be explained by the shrinking and swelling of expansive clay, also known as Yazoo clay, which is prevalent in the central Mississippi region. Yazoo clay has significant shrinkage and swelling with changing wetting and drying weather patterns, causing ground movements.

Some limitations include less control over error explanation and mitigation in InSAR analysis. Furthermore, the InSAR ground displacement raster cell sizes had a low resolution of 30' x 30'. In contrast, the displacements obtained from LiDAR and UAV time-series DEMs were at centimeter levels, thus making comparing the InSAR and high-resolution LiDAR DEMs challenging.

Nonetheless, the method proved an excellent tool for preemptively identifying at-risk geotechnical assets such as highway embankment slopes, dams, and levees. Future studies will

focus on delineating the translational and vertical displacements from InSAR results and continue further comparisons with high-resolution LiDAR DEM observations to explore more agreeable comparisons. In addition, future research will use this comprehensive dataset to develop finite-element-based numerical models, which will help create surrogate models for highway embankment assets that match the ground motion patterns observed in InSAR analysis. This study will be a foundation for developing machine learning classification models incorporating features and targets from InSAR and LiDAR observations.

ACKNOWLEDGMENTS

The research presented in this study was partially supported by the National Science Foundation (NSF) projects CMMI #2152896, CMMI# 2046054, and State Study 316, funded by the Mississippi Department of Transportation (MDOT). The authors sincerely appreciate the support of the grants for this study. This paper's contents, statements, and views are strictly those of the authors and do not necessarily reflect the views of their affiliates or the funding agencies.

REFERENCES

Akcin, H., H. S. Kutoglu, H. Kemaldere, T. Deguchi, and E. Koksal. "Monitoring Subsidence effects in the Urban Area of Zonguldak Hardcoal Basin of Turkey by InSAR-GIS Integration." *Natural Hazards and Earth System Sciences* 10, no. 9 (September 1, 2010): 1807–14.

Berardino, P., G. Fornaro, R. Lanari, and E. Sansosti. "A New Algorithm for Surface Deformation Monitoring Based on Small Baseline Differential SAR Interferograms." *IEEE Trans. Geosci. Remote. Sens.* 40 (2002): 2375–83.

Chan, Y.-C., Y.-G. Chen, T.-Y. Shih, and C. Huang. "Characterizing the Hsincheng Active Fault in Northern Taiwan Using Airborne LiDAR Data: Detailed Geomorphic Features and Their Structural Implications." *Journal of Asian Earth Sciences* 31, no. 3 (November 2007): 303–16.

Ferretti, A., C. Prati, and F. Rocca. "Permanent Scatterers in SAR Interferometry." *IEEE Transactions on Geoscience and Remote Sensing* 39, no. 1 (2001): 8–20.

Fruneau, B., J. Achache, and C. Delacourt. "Observation and Modelling of the Saint-Étienne-de-Tinée Landslide Using SAR Interferometry." *Tectonophysics* 265, no. 3–4 (November 1996): 181–90.

Herrera, G., R. Tomás, F. Vicente, J. M. Lopez-Sanchez, J. J. Mallorquí, and J. Mulas. "Mapping Ground Movements in Open Pit Mining Areas Using Differential SAR Interferometry." *International Journal of Rock Mechanics and Mining Sciences* 47, no. 7 (October 2010): 1114–25.

Lauknes, T. R. "Long-Term Surface Deformation Mapping Using Small-Baseline Differential SAR Interferograms," 2004. https://api.semanticscholar.org/CorpusID:12348152.

Massonnet, D., and K. L. Feigl. "Radar Interferometry and Its Application to Changes in the Earth's Surface." *Reviews of Geophysics* 36, no. 4 (November 1998): 441–500.

Downloaded from ascelibrary.org by A Q M Zohuruzzaman on 04/23/25. Copyright ASCE. For personal use only; all rights reserved.